Received: 5 January 2024 | Revised: 17 April 2024 | Accepted: 28 April 2024

DOI: 10.1111/jnc.16127

Journal of Neurochemistry JNC The Official Journal of the International Society for Neurochemistry WILEY

ORIGINAL ARTICLE

Antibody engagement with amyloid-beta does not inhibit [^{11}C]PiB binding for PET imaging

Mengfei Xiong[1] | Amelia Dahlén[1] | Sahar Roshanbin[1] | Elin Wik[1] | Ximena Aguilar[1] | Jonas Eriksson[2,3] | Dag Sehlin[1] | Stina Syvänen[1]

[1]Molecular Geriatrics, Department of Public Health and Caring Sciences, Uppsala University, Uppsala, Sweden

[2]Department of Medicinal Chemistry, Uppsala University, Uppsala, Sweden

[3]PET Centre, Uppsala University Hospital, Uppsala, Sweden

Correspondence
Stina Syvänen, Molecular Geriatrics, Department of Public Health and Caring Sciences, Uppsala University, SE-751 85 Uppsala, Sweden.
Email: stina.syvanen@pubcare.uu.se

Funding information
Gun och Bertil Stohnes Stiftelse; Konung Gustaf V:s och Drottning Victorias Frimurarestiftelse; Stiftelsen för Gamla Tjänarinnor; Magnus Bergvalls Stiftelse; Åhlén-stiftelsen; Hjärnfonden; Alzheimerfonden; Vetenskapsrådet, Grant/Award Number: 2021-01083 and 2021-03524

Abstract

The elimination of amyloid-beta (Aβ) plaques in Alzheimer's disease patients after treatment with anti-Aβ antibodies such as *lecanemab* and *aducanumab* is supported by a substantially decreased signal in amyloid positron emission tomography (PET) imaging. However, this decreased PET signal has not been matched by a similar substantial effect on cognitive function. There may be several reasons for this, including short treatment duration and advanced disease stages among the patients. However, one aspect that has not been investigated, and the subject of this study, is whether antibody engagement with amyloid plaques inhibits the binding of amyloid-PET ligands, leading to a false impression of Aβ removal from the brain. In the present study, tg-ArcSwe mice received three injections of RmAb158, the murine version of *lecanemab* or phosphate-buffered saline (PBS) before the administration of the amyloid-PET radioligand [^{11}C]PiB, followed by isolation of brain tissue. Autoradiography showed that RmAb158- and PBS-treated mice displayed similar [^{11}C]PiB binding. Moreover, the total Aβ1–40 levels, representing the major Aβ species of plaques in the tg-ArcSwe model, as well as soluble triggering receptor on myeloid cells 2 (sTREM2) levels, were similar in both groups. Interestingly, the concentration of soluble Aβ aggregates was decreased in the RmAb158-treated group, along with a small but significant decrease in the total Aβ1–42 levels. In conclusion, this study indicates that the binding of [^{11}C]PiB to Aβ accurately mirrors the load of Aβ plaques in the brain, aligning with how amyloid-PET is interpreted in clinical studies of anti-Aβ antibodies. However, early treatment effects on soluble Aβ aggregates and Aβ1–42 levels were not detected.

KEYWORDS
[^{11}C]PiB, Alzheimer's disease (AD), amyloid-beta, amyloid PET, antibody treatment, immunotherapy

Abbreviations: ^{11}C, carbon-11; ^{18}F, fluorine-18; AD, Alzheimer's disease; APP, amyloid precursor protein; Aβ, amyloid-beta; BBB, blood–brain barrier; Cat, catalogue number; ELISA, enzyme-linked immunosorbent assay; FA, formic acid; FDA, Food and Drug Administration; PBS, phosphate-buffered saline; PET, positron emission tomography; RRID, Research Resource Identifier; sTREM2, soluble triggering receptor on myeloid cells 2; TBS, tris-buffered saline; TfR, transferrin receptor; Tg, transgenic; ThS, thioflavin-S; ThT, thioflavin-T.

1 | INTRODUCTION

Immunotherapy, that is, antibody treatment, directed towards amyloid-beta (Aβ) aggregates, is currently the most promising strategy for treating Alzheimer's disease (AD). In 2023, the U.S. Food and Drug Administration (FDA) approved the anti-Aβ antibody *lecanemab* after clinical phase III data showed 27% less cognitive decline in patients treated biweekly with 10 mg/kg of the antibody compared to the control group (van Dyck et al., 2023). Late phase clinical trials with antibodies *aducanumab* and *donanemab* also demonstrated slower cognitive decline in patients treated with the antibodies compared to placebo-treated patients (Budd Haeberlein et al., 2022; Sims et al., 2023). Moreover, biomarker data have had a crucial role in the approvals and conditional approvals of these three antibodies. For example, positron emission tomography (PET) imaging has been used extensively to assess the ability of anti-Aβ antibodies to reduce brain amyloid during the treatment periods.

Several amyloid PET imaging radioligands are available for this purpose. Among these radioligands, the thioflavin-derived carbon-11 (^{11}C) radiolabelled [^{11}C]PiB was the first to be used, while later FDA-approved radioligands include benzothiazole derivatives and fluorine-18 (^{18}F) radiolabelled [^{18}F]flutemetamol (Nelissen et al., 2009), [^{18}F]florbetaben (Rowe et al., 2008) and [^{18}F]florbetapir (Clark et al., 2011). These PET radioligands, along with fluorescent dyes thioflavin-T (ThT) and thioflavin-S (ThS), are widely used for studying protein aggregation in vitro and ex vivo. They bind primarily to amyloid structures found predominantly in fibrillar forms of Aβ (Frieg et al., 2020; Ikonomovic et al., 2008), although weaker binding to diffuse Aβ pathology is also present (Ikonomovic et al., 2020). It should be noted that many proteins other than Aβ can form amyloid structures, so the amyloid-PET radioligands, as well as fluorescent dyes ThT and ThS, are not specific for Aβ but can also bind to other aggregated proteins such as alpha-synuclein and tau fibrils (Mishra et al., 2020; Roshanbin et al., 2022; Tao et al., 2023; Ye et al., 2008). However, despite frequent co-pathology presence in the AD brain (Alafuzoff & Libard, 2020), it remains unclear if amyloid radioligand binding to aggregates of other proteins than Aβ contributes to the in vivo PET signal.

PET imaging has convincingly and consistently demonstrated that the signal with amyloid radioligands is dramatically reduced in a dose-dependent manner after treatment with anti-Aβ antibodies (Budd Haeberlein et al., 2022; Liu et al., 2015; Lowe et al., 2021; Rinne et al., 2010; Sevigny et al., 2016; Sims et al., 2023; Swanson et al., 2021; van Dyck et al., 2023). This outcome has been interpreted as the successful removal of brain amyloid, which likely comprises insoluble aggregated Aβ, that is, Aβ plaques. In the highest antibody dose groups (10–50 mg/kg), PET signals have been reported to decrease below the set threshold for pathological levels of amyloid after 12–18 months of treatment, and PET images obtained at these time points have even become comparable to healthy, age-matched controls. However, this pronounced decrease in brain amyloid, as indicated by a reduced amyloid PET signal, has not been accompanied by a corresponding dramatic improvement in cognitive performance. In fact, patients continue to experience cognitive decline, albeit at a slower rate, despite antibody treatment. One explanation might be found in the secondary damages caused by Aβ aggregation (Figure 1a), which involve tau hyperphosphorylation and aggregation, chronic inflammation and neuronal degeneration. Consequently, the removal of brain Aβ may not immediately inhibit these pathological processes, especially if the antibody treatment has been initiated well into disease progression. However, the discrepancy between the continuation of cognitive decline and the dramatically reduced PET signal raises the question of whether the reduced PET signals truly reflect the removal of Aβ or if antibody administration merely inhibits the binding of PET amyloid radioligands to their target, potentially leading to an overestimation of the magnitude of Aβ removal. Thus, this study aimed to investigate whether the administration of RmAb158, the murine antibody version of *lecanemab*, can indeed block the binding of the amyloid PET radioligand [^{11}C]PiB.

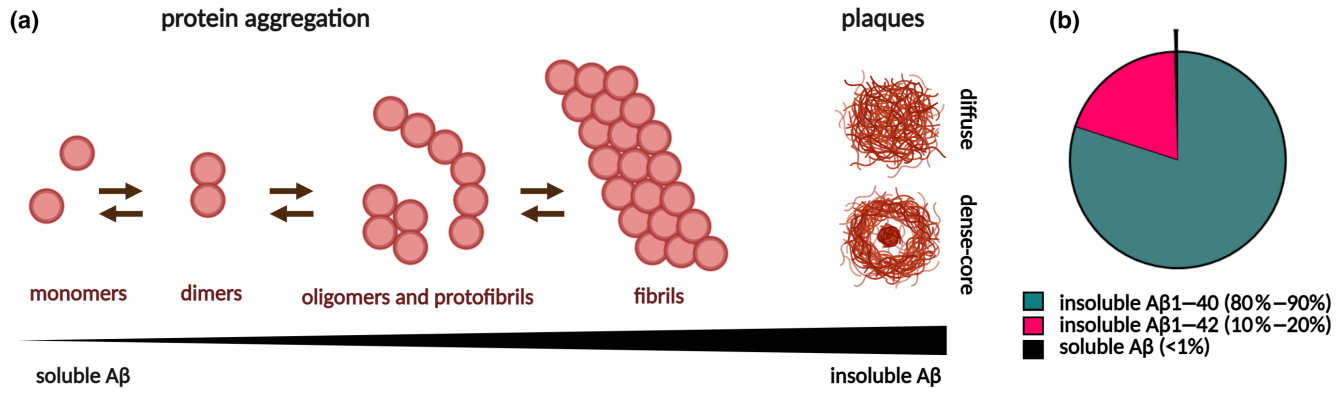

FIGURE 1 Aggregation of amyloid-beta (Aβ). (a) When misfolding, Aβ monomers may aggregate into dimers, oligomers and protofibrils, and eventually form fibrils that can be deposited as amyloid plaques with or without a dense core. The aggregates become gradually insoluble with increased size. (b) The Aβ pathology in the tg-ArcSwe model used in the present study is composed of both Aβ1–40 and Aβ1–42, with the majority being found as insoluble deposited aggregates. This includes dense-core plaques, which contain a large amount of tightly packed Aβ fibrils that form the primary Aβ structure detected by amyloid-PET radioligands (a: created with BioRender software).

2 | METHODS

2.1 | Mice

Transgenic mice (tg-ArcSwe) bred in-house, harbouring the human amyloid precursor protein (APP) gene with the Arctic (E693G) and Swedish (KM670/671NL) mutations, were used throughout the study. This mouse model is characterized by a gradual deposition of aggregated Aβ that begins at 6–7 months (Lord, Englund, et al., 2009; Magnusson et al., 2013). In contrast to many other mouse models of AD pathology that predominantly display Aβ1–42 pathology, tg-ArcSwe mice have deposits of both Aβ1–40 and Aβ1–42 (Figure 1b). Additionally, tg-ArcSwe mice form human-like plaques with a dense core primarily consisting of aggregated insoluble Aβ fibrils (Zielinski et al., 2023). It is believed that amyloid radioligands primarily bind to the amyloid in the dense core of the deposits. Thus, the utilization of the tg-ArcSwe model is particularly well suited for studies involving amyloid-PET radioligands, whereas many other frequently used animal models of AD develop mostly diffuse Aβ pathology with deposits without or with a very small dense core. Consequently, these models only exhibit weak amyloid-PET positivity (Syvänen et al., 2022). All tg-ArcSwe mice used in the experiments were 19–21 months old ($n=22$). At this age, tg-ArcSwe mouse brains contain abundant Aβ pathology that is detectable by [^{11}C]PiB PET imaging in line with the presence of large ThS-positive Aβ deposits (Fang et al., 2019; Meier et al., 2022; Sehlin et al., 2016). In addition to tg-ArcSwe mice, four wild-type (WT) littermate mice were included for the comparison of amyloid-PET radioligand [^{11}C]PiB concentrations in brain and blood. Both males (33 ± 3 g) and females (27 ± 4 g) were used, and the mice had *ad libitum* access to food and water and were kept under a 12/12-h light/dark cycle. They were housed in groups of three to five mice in Makrolon type III cages (Tecniplast Inc., Italy). Occasionally, male mice had to be single-housed because of aggressive behaviour. All experimental procedures were approved by the Uppsala County Animal Ethics board (5.8.18–20401/2020), conducted according to regulations of the Swedish Animal Welfare Agency, and in compliance with the European Communities Council Directive of 22 September 2010 (2010/63/EU). All experiments were conducted in compliance with the ARRIVE guidelines. All analyses, except autoradiography and ex vivo measurement of radioactivity, were performed blinded, that is, the person who carried out the experimental procedure had no information of whether a specific mouse belonged to the RmAb158- or PBS-treated group.

2.2 | Antibody treatment and [^{11}C]PiB administration

The recombinant murine version of the anti-Aβ antibody *lecanemab*, RmAb158, was produced in-house as previously described (Fang et al., 2017; Gustavsson et al., 2023). Tg-ArcSwe mice were administered three intravenous (i.v.) injections of 50 mg/kg RmAb158 ($f=7$, $m=4$) or phosphate-buffered saline (PBS, $f=7$, $m=4$) over 2 weeks. Allocation to the two different treatment groups was based on the breeding cage from which the mouse originated and gender, with the aim of including mice from each breeding cage and balancing males and females in both groups. No formal sample size calculation was performed a priori. Instead, group sizes ($n=11$) were based on previous studies of similar characters which have shown that given the variation in pathology among tg-ArcSwe mice, group sizes of 8–12 mice are required to detect 20% differences between treatment groups (Meier et al., 2018, 2022; Rofo et al., 2022). Failed i.v. injections of RmAb158 were an exclusion criterion; however, no such event occurred.

The radioligand [^{11}C]PiB was produced according to a published method (Solbach et al., 2005). The molar activity was 369.3 ± 45.7 GBq/μmol at the end of the synthesis. All mice received the same molar amount of [^{11}C]PiB by i.v. administration, corresponding to 10.8 ± 4.1 MBq, 3 days after the last RmAb158 or PBS treatment. All i.v. administrations were done under light anaesthesia using 2% isoflurane (Baxter International Inc., Deerfield, IL, USA) in medical air supplemented with oxygen gas (0.2 L/min). One mouse in each treatment group did not receive [^{11}C]PiB but was kept in the study for analyses of brain Aβ and soluble triggering receptor on myeloid cells 2 (sTREM2) levels. Four WT mice (untreated, $f=3$, $m=1$) also received [^{11}C]PiB. Mice were killed at 40 min after the [^{11}C]PiB injection by decapitation under deep isoflurane anaesthesia using 4–5% isoflurane in medical air, a blood sample was obtained, and the brain was immediately isolated and frozen.

2.3 | Ex vivo autoradiography and ThS staining

Three 20-μm sagittal brain sections per mouse were prepared from the right hemisphere and mounted on anti-freeze glass. After drying, sections were transferred to a phosphor imaging plate (BAS-IP SR 2040, Fujifilm, product # 28956477) at 20 min post-killing, and were exposed for 90 min at room temperature alongside a radioactivity standard (Bq/mL). After exposure, plates were scanned in an Amersham Typhoon IP phosphor imager (GE Healthcare, product #29187194) at a resolution of 100 μm. Images were calibrated according to the radioactivity standard and molar activity. One region of interest was drawn in the cerebrum and one in the cerebellum of each brain section. The binding of [^{11}C]PiB in the respective region was calculated from the raw images in greyscale and then expressed as fmol/mg wet tissue weight. Finally, the images were converted to a false colour scale (Royal) in ImageJ (Fiji 1.53t, USA, RRID:SCR_003070). Consecutive brain sections to those used for autoradiography for a subset of mice were used for ThS staining. Sections were dried completely at room temperature, fixed in 70% ethanol, and washed in MiliQ water for 1 min each, followed by incubating with 0.5 mM ThS (product # T1892, Sigma-Aldrich) aqueous solution for 15 min. Sections were washed in decreasing concentrations of ethanol (80%–70%–0%) for 1 min and mounted with EverBrite Hardset Mounting Medium with DAPI (Cat # 23004, Biotium, Hayward, CA). The staining was imaged at 10× and 40× with a Zeiss Axio Observer Z.1 microscope (RRID:SCR_021351) and

ZEN 2.6 software (Carl Zeiss Microimaging GmbH, Jena, Germany). Summed punctate staining in the cortex ($8 \times 0.42\,mm^2$), hippocampus ($3 \times 0.24\,mm^2$), thalamus ($1.76\,mm^2$) and cerebellum ($1.76\,mm^2$) were counted in ImageJ using Analyse Particles (size: 110-infinity) after thresholding.

2.3.1 | Determination of radioactivity

Radioactivity in the blood and left hemisphere brain samples was measured in a γ-counter (2480 Wizard™, PerkinElmer, Waltham, USA). Brain activity was presented as a standardized uptake value (SUV), which was calculated using the following equation:

$$SUV = \frac{\text{Radioactivity (kBq) / tissue weight (g)}}{\text{Injected activity (MBq) / body weight (kg)}}.$$

2.4 | Brain homogenization

The isolated brain was extracted in a 1:10 tissue weight/extraction volume ratio (w/v) with tris-buffered saline (TBS, pH 7.6), which contained 20 mmol/L Tris (product # 1.08382.1000, Merck Millipore) and 137 mmol/L NaCl (product # 1.06404.1000, Supelco) including a complete protease inhibitor cocktail (product # 04693124001, Roche). This extraction was performed using a Precellys® Evolution homogenizer (product # S002274-PEVO0-A.0, Bertin Technologies, France) at 5500 rpm (4×10 s with a 30-s break in between). The homogenates were first centrifuged at 16 000 *g* at 4°C for 60 min. The supernatant was isolated and an aliquot was subsequently centrifuged at 100 000 *g* at 4°C for 60 min. Again, the supernatant was isolated to obtain an extract containing the soluble Aβ aggregates (Gustavsson et al., 2023; Syvänen et al., 2018). This TBS extract was also used for the analysis of sTREM2. The pellet that remained after the 16 000 *g* centrifugation was re-extracted in 70% formic acid (FA, product # 695076, Sigma-Aldrich) with a 1:10 (w/v) ratio and centrifuged at 16 000 *g* at 4°C for 60 min. The supernatant, which contained the fibrillar Aβ species present in the insoluble Aβ brain deposits, was collected. The supernatants were stored at −20°C until ELISA measurements.

2.5 | ELISA to determine concentrations of soluble Aβ aggregates, Aβ40, Aβ42 and sTREM2

Assessments of soluble Aβ aggregates, total Aβ40 and Aβ42 and sTREM2 with ELISA were conducted as previously described (Gustavsson et al., 2023; Meier et al., 2021; Syvänen et al., 2018). All samples were analysed in triplicates. Briefly, the concentrations of soluble Aβ aggregates were determined in the brain TBS extracts using a sandwich ELISA based on the Aβ N-terminal-specific antibody 3D6 (produced in-house) as both capture and detection antibody. This ELISA will detect Aβ aggregates from the size of a dimer to larger aggregates. Ninety-six-well half-area plates (product # CLS3690, Corning Inc. Corning, NY, USA) were coated with 50 ng of 3D6 per well overnight at +4°C, then blocked for 2 h with 1% bovine serum albumin (BSA, product # A7030, Sigma-Aldrich). Brain TBS extracts were incubated overnight at +4°C and then detected with biotinylated 3D6 and streptavidin-HRP (product # 3310–9-1000, Mabtech, Nacka Strand, Sweden). The ELISA was developed with K-blue Aqueous TMB substrate (product # 331175, Neogen Corp., Lexington, KY, USA) and read with a spectrophotometer at 450 nm. Samples were quantified against a calibration standard curve of Aβ protofibrils, prepared by size exclusion chromatography purification of Aβ1–42 (cat # SP-BA42-1, Innovagen, Lund, Sweden) after 3-h incubation at 37°C. Total brain concentrations of Aβ1–40 and Aβ1–42 were analysed in the FA brain extracts. Briefly, two 96-well plates were coated overnight with polyclonal rabbit anti-Aβ40 (custom production, Agrisera, Umeå, Sweden) and monoclonal anti-Aβ42 antibody clone H31L21 (product # 700254, Invitrogen, Sweden, RRID:AB_2532306), respectively, then blocked with 1% BSA. The FA brain extracts were neutralized with 2 M Tris and diluted in ELISA incubation buffer, then incubated on the plate overnight at +4°C and detected with biotinylated 3D6 and streptavidin-HRP as above. Levels of sTREM2 in the TBS brain extract were analysed with a sandwich ELISA. First, plates were coated with polyclonal anti-mouse TREM2 antibody (cat # AF1729, R&D, Abingdon, UK, RRID:AB_354956) (20 ng per well) overnight at 4°C, then blocked with 1% BSA. Brain extracts were added, incubated overnight at 4°C and detected with a 3-h incubation of biotinylated anti-mouse TREM2 antibody (cat # BAF1729, R&D, RRID:AB_356109) and 2 h with streptavidin-HRP as above.

2.6 | Statistical analysis

All analyses were performed with GraphPad Prism 9.4.1 (GraphPad Software, San Diego, USA). Results are reported as mean ± SD. Comparisons between [^{11}C]PiB retention in the RmAb158- and the PBS-treated tg-ArcSwe and the untreated WT groups were conducted using a one-way ANOVA with correction for multiple comparisons using the Sidak–Holm method. Comparisons between autoradiography-based [^{11}C]PiB binding, Aβ and sTREM2 levels in the RmAb158- and the PBS-treated groups were conducted using unpaired t-tests. The number of ThS-positive plaques in the RmAb158- and the PBS-treated groups was compared using a two-way ANOVA (group and brain region as variables), with correction for multiple comparisons using the Sidak method. Pearson correlation tests (*r*) and simple linear regression (R^2) were employed to analyse the correlation between ELISA measurements and the [^{11}C]PiB binding. All tests were two-tailed, and the significance level was set to 95%, indicated as $^*p < 0.05$, $^{**}p < 0.01$, $^{***}p < 0.001$, ns: $p > 0.05$. All data were also assessed for normal distribution using the Shapiro–Wilk test at a significance level of 0.05. The results indicated that the data were normally distributed across all groups. The ROUT outlier test was used. Details of all statistical tests are given in the Supporting Information.

3 | RESULTS

3.1 | In vivo blocking of [^{11}C]PiB with RmAb158

Tg-ArcSwe mice were treated with three i.v. injections of either RmAb158 or PBS during 2 weeks before [^{11}C]PiB administration. High [^{11}C]PiB binding was found in the cerebral cortex, hippocampus and interbrain (thalamus and hypothalamus), while moderate binding was detected in the striatum and cerebellum (Figure 2a; Figure S1). No differences in [^{11}C]PiB binding, as measured by autoradiography, were observed between the RmAb158-treated and PBS-treated mice (Figure 2b). In PET, the binding in the region of interest is often normalized to the binding in a reference region that is devoid of pathology. Thus, a ratio between the binding in the cerebrum and cerebellum was also generated. However, there was no difference in this ratio between the two treatment groups (Figure 2c). In line with the autoradiography, [^{11}C]PiB brain concentrations measured by γ-counting did not differ between the RmAb158-treated and PBS-treated mice (Figure 2d). The SUV ratio (SUVR), the primary outcome measure in clinical studies, as well as the brain-to-blood concentration ratio that takes into account potential differences in systemic elimination of the radioligand, were also similar in both treatment groups. However, these ratios were notably elevated in the tg-ArcSwe compared to WT mice demonstrating that [^{11}C]PiB was indeed retained in the tg-ArcSwe brain because of the engagement with Aβ pathology (Figure 2e,f).

3.2 | Aβ concentrations in brain extracts

The analysis of different Aβ pools in the brain—namely, soluble Aβ aggregates, and total Aβ1–40 and Aβ1–42—revealed a 33% decrease in the concentration of TBS soluble Aβ aggregates in the RmAb158-treated group compared to the PBS-treated control group (Figure 3a). There was no difference in total Aβ1–40 concentrations

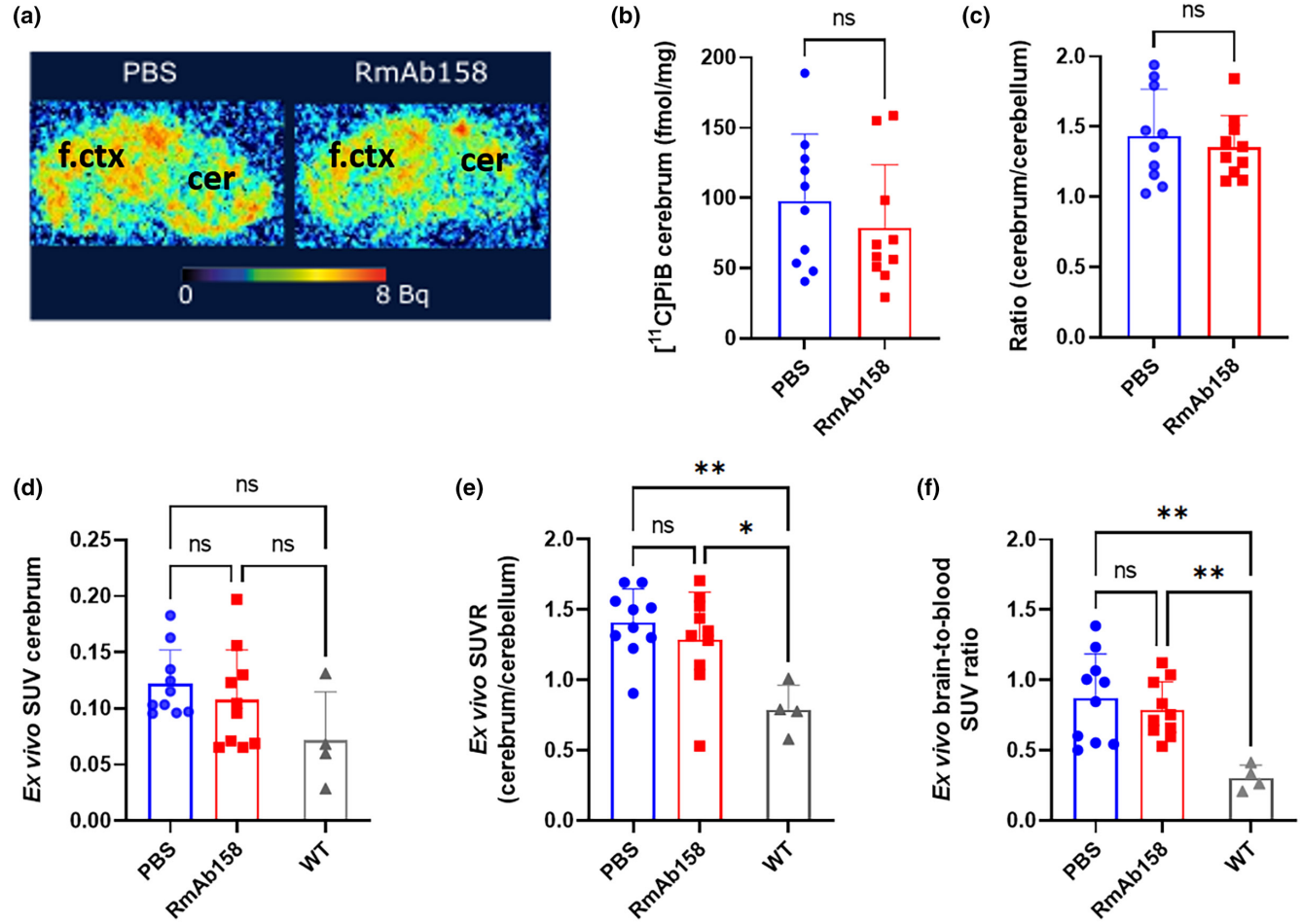

FIGURE 2 Binding of amyloid-PET radioligand [^{11}C]PiB was the same in RmAb158- and phosphate-buffered saline (PBS)-treated mice. (a) Example of ex vivo autoradiography images of sagittal brain sections prepared from mice killed 40 min after [^{11}C]PiB injection (cer, cerebellum; f.ctx, frontal cortex). (b) [^{11}C]PiB binding expressed as fmol/mg wet tissue weight quantified by autoradiography on brain sections in the cerebrum. (c) The [^{11}C]PiB binding ratio between cerebrum and cerebellum based on autoradiography. (d) Body weight and dose normalized [^{11}C]PiB brain concentrations expressed as SUV based on γ-counting. (e) The SUV ratio (SUVR) based on the SUV in the cerebrum and in the cerebellum. (f) The concentration ratio based on the SUV in the cerebrum and in the blood. SUV, standardized uptake value. Blue circular symbols represent PBS-treated tg-ArcSwe mice ($n = 10$), red square symbols represent RmAb158-treated tg-ArcSwe mice ($n = 10$), grey triangle symbols represent untreated wild-type (WT) mice ($n = 4$). $^{*}p < 0.05$, $^{**}p < 0.01$, $^{***}p < 0.001$, ns: $p > 0.05$.

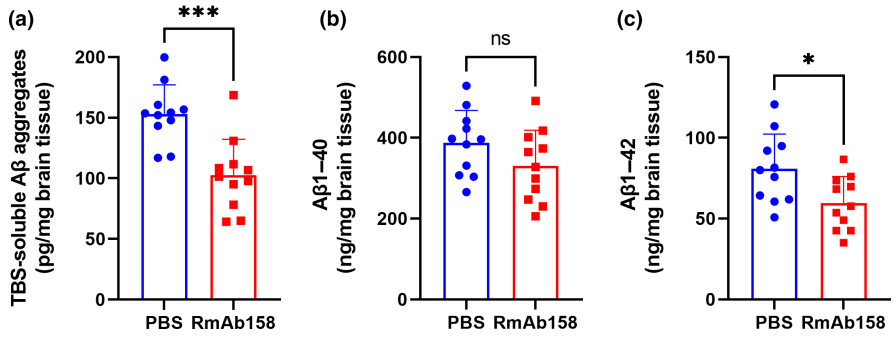

FIGURE 3 Aβ concentrations in brain tissue. (a) Soluble amyloid-beta (Aβ) aggregates measured in TBS extracts obtained after 100000 g centrifugation were decreased in the group of tg-ArcSwe mice that had been treated with RmAb158 compared to the control phosphate-buffered saline (PBS)-treated tg-ArcSwe mice. (b) Aβ1–40 concentrations in the formic acid (FA) brain extracts were similar in RmAb158 or PBS-treated tg-ArcSwe mice. (c) RmAb158-treated mice showed decreased Aβ1–42 concentrations in FA brain extracts. Blue circular symbols represent PBS-treated mice ($n = 11$), while red square symbols represent RmAb158-treated mice ($n = 11$). TBS, tris-buffered saline. $^{*}p < 0.05$, $^{***}p < 0.001$, ns: $p > 0.05$.

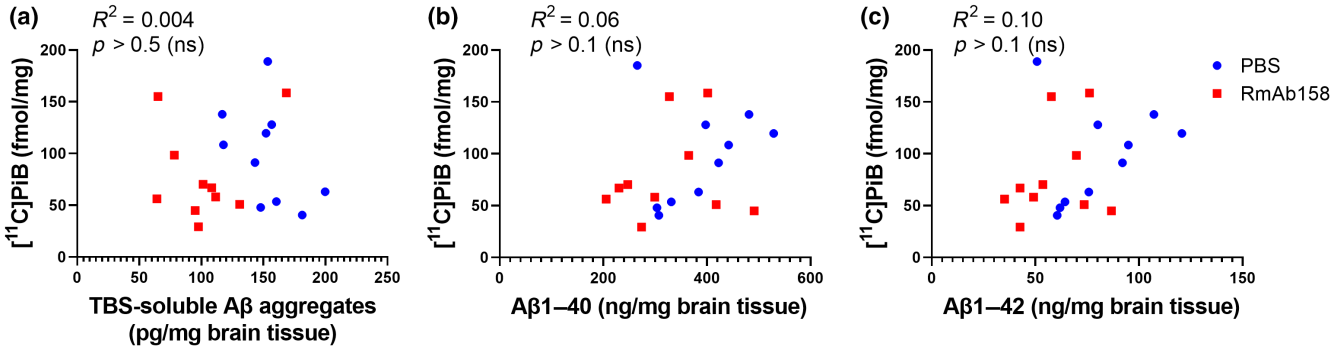

FIGURE 4 No significant correlation between [^{11}C]PiB binding to brain tissue sections and (a) soluble amyloid-beta (Aβ) aggregates, (b) Aβ1–40 or (c) Aβ1–42 concentrations was detected. Blue circular symbols represent phosphate-buffered saline-treated tg-ArcSwe mice ($n = 10$), while red square symbols represent RmAb158-treated tg-ArcSwe mice ($n = 10$). TBS, tris-buffered saline.

(Figure 3b), which are likely to correspond to plaque-deposited Aβ relevant for [^{11}C]PiB binding. Interestingly, a decrease in Aβ1–42 levels was also observed in the RmAb158-treated group (Figure 3c).

The relatively high variation in Aβ pathology among animals was anticipated, as mice of this age are known to exhibit varying Aβ load. The diversity in Aβ levels among mice allowed for a direct correlation between [^{11}C]PiB binding and a range of Aβ concentrations. However, no significant correlation between [^{11}C]PiB binding and Aβ concentrations was observed, regardless of whether the correlation analysis was conducted separately within the two treatment groups or across all mice (Figure 4).

3.3 | ThS staining

ThS staining revealed pathology similar to what has previously been described for the tg-ArcSwe model (Meier et al., 2018), that is, plaques were mainly located in the cortex, hippocampus and thalamus, while scattered staining was found in the dorsal striatum and cerebellar cortex. In the cortex and thalamus, the staining was relatively universal. In the hippocampus, the staining was primarily distributed in the subiculum, the Cornu Ammonis 3 (CA3) and the dentate gyrus subregions. The number of deposits did not differ between PBS- and RmAb158-treated animals in any of the studied regions (Figure S2).

3.4 | sTREM2 concentrations in brain extracts

There was no difference in microglial marker sTREM2 concentration between RmAb158- and PBS-treated mice (Figure 5). However, there was a significant positive correlation between Aβ1–40 and sTREM2 levels, as well as between Aβ1–42 and sTREM2 levels. When treatment groups were analysed separately, this correlation was only significant for the RmAb158-treated group. There was no correlation between soluble Aβ aggregates and sTREM2.

4 | DISCUSSION

Amyloid PET has become an important tool in clinical trials of new antibodies aimed at removing Aβ from the AD brain. Today, PET is not only used as an inclusion criterion to ensure that strictly amyloid

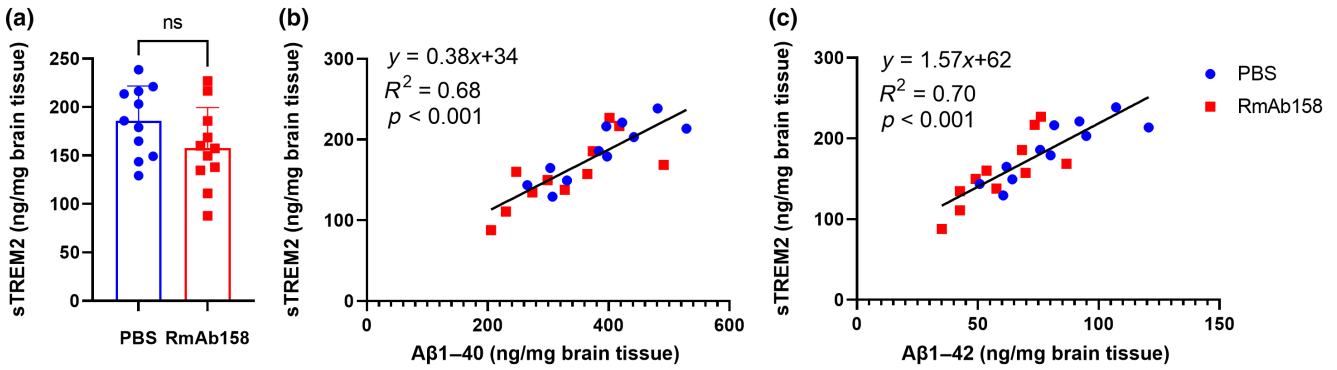

FIGURE 5 Soluble triggering receptor on myeloid cells 2 (sTREM) concentrations in tris-buffered saline (TBS) brain extracts. (a) sTREM2 measured in TBS-extracts were similar in RmAb158- and phosphate-buffered saline (PBS)-treated tg-ArcSwe mice. (b) A positive correlation was found between Aβ1–40 and sTREM levels. (c) A positive correlation was also found between Aβ1–42 and sTREM levels (in b, c: PBS- and RmAb158-treated tg-ArcSwe mice analysed together). Blue circular symbols represent PBS-treated mice ($n = 11$), while red square symbols represent RmAb158-treated mice ($n = 11$).

positive patients are enrolled in clinical trials but also to evaluate the effects of therapeutic antibodies. Several studies have demonstrated that antibody treatment reduces the PET signal obtained with amyloid-binding PET radioligands, such as [^{11}C]PiB, [^{18}F]flutemetamol and [^{18}F]florbetapir (Budd Haeberlein et al., 2022; Liu et al., 2015; Lowe et al., 2021; Rinne et al., 2010; Sevigny et al., 2016; Sims et al., 2023; Swanson et al., 2021; van Dyck et al., 2023). Further, a few case studies using post-mortem brain tissue isolated from patients treated with anti-Aβ antibodies have provided indications that the treatment has promoted Aβ phagocytosis, most likely by microglia (Castellani et al., 2023; Plowey et al., 2022). In theory, Aβ antibodies and amyloid-PET radioligands should not bind to the same binding site. For example, RmAb158 binds to the N-terminal part of Aβ (Englund et al., 2007), while [^{11}C]PiB binds to the cavity formed by cross-β structures in Aβ deposits (Englund et al., 2007; Peccati et al., 2017). Accordingly, with different binding sites, no blocking of binding between the two classes of molecules is expected to occur. Still, no study so far has explicitly showed that antibody engagement with Aβ plaques does not hinder the access of amyloid-PET radioligands to their binding sites. In this study, we show that such blocking is unlikely to occur.

The study was designed to attain high RmAb158 concentrations in the brain within a short time frame. The dose of 50 mg/kg was based on previous studies in tg-ArcSwe mice that have demonstrated RmAb158 engagement with brain Aβ from 3 days, when brain antibody concentrations peak, up to at least 2 weeks post-administration (Gustavsson et al., 2020; Magnusson et al., 2013; Syvänen et al., 2018). The goal was to ensure that the actual removal of brain Aβ deposits would not have sufficient time to occur, but the binding of antibodies to plaques would be maximized. This objective was largely achieved, as total concentrations of Aβ1–40, the primary component of insoluble plaques in the tg-ArcSwe model, remained at the same level in the RmAb158-treated mice compared to the PBS group. Also, sTREM2 levels were similar in both groups indicating that the antibody did not substantially activate microglia phagocytosis of Aβ, that is, the mechanism through which brain Aβ is believed to be cleared by immunotherapy. Previous studies have shown that long-term antibody treatment results in increased sTREM2, while low Aβ pathology in tg-ArcSwe mice is linked to low sTREM2 levels (Gustavsson et al., 2023; Meier et al., 2021, 2022). Consistent with this, a positive correlation between Aβ pathology and sTREM2 was also observed in the present study. The decrease in the pool of soluble Aβ aggregates, often termed Aβ protofibrils, serves as an indication of a therapeutic effect. These Aβ species are considered the primary target of RmAb158, as well as the humanized and FDA-approved *lecanemab* (Englund et al., 2007; Söderberg et al., 2023). This reduction was consistent with previous immunotherapy studies conducted in animal models of Aβ pathology (Lord, Gumucio, et al., 2009; Syvänen et al., 2018; Tucker et al., 2015). Perhaps somewhat less expected, RmAb158 treatment also led to a reduction in total Aβ1–42. In tg-ArcSwe mice, Aβ1–42 is typically located at the borders, often referred to as the 'halo', of the insoluble Aβ plaques. Thus, RmAb158 is more likely to initially interact with Aβ1–42 than with Aβ1–40, primarily because of greater accessibility. One limitation in the quantification of the various Aβ species and sTREM2 in this study lies in utilizing in-house ELISA assays. Nonetheless, since all samples were analysed on the same plate, comparative assessments between mice can be considered consistent. In clinical studies, antibody treatments have been conducted over much longer periods than the 3 weeks used in the present study. However, it is important to note that the present study demonstrates that early treatment effects, such as removal of Aβ protofibrils and diffuse Aβ42 pathology, are unlikely to be detected by amyloid-PET imaging. In fact, the present study revealed no significant correlation between Aβ concentrations and [^{11}C]PiB binding, indicating that amyloid-PET is a relatively 'blunt' tool for the measurement of pathology at the individual level. This corroborates our previous studies showing that PET radioligands based on anti-Aβ antibodies are superior to [^{11}C]PiB in detecting the early effects of Aβ-lowering drugs (Meier et al., 2018, 2022; Sehlin & Syvanen, 2019).

In summary, the present study supports the validity of the interpretation that a reduced amyloid-PET signal, as reported in clinical studies of anti-Aβ antibodies, reflects a reduced brain Aβ burden. It also highlights the shortcomings of amyloid PET in detecting early treatment effects on certain Aβ species, such as Aβ protofibrils, which are the main targets of *lecanemab*.

AUTHOR CONTRIBUTIONS

Mengfei Xiong: Conceptualization; investigation; formal analysis; writing – original draft; writing – review and editing. **Amelia Dahlén:** Investigation; writing – review and editing. **Sahar Roshanbin:** Investigation; writing – review and editing. **Elin Wik:** Investigation; writing – review and editing. **Ximena Aguilar:** Investigation; writing – review and editing. **Jonas Eriksson:** Writing – review and editing. **Dag Sehlin:** Conceptualization; investigation; writing – review and editing; funding acquisition. **Stina Syvänen:** Conceptualization; investigation; formal analysis; writing – original draft; writing – review and editing; funding acquisition; supervision.

ACKNOWLEDGMENTS

The molecular imaging work in this study was performed at the SciLifeLab Pilot Facility for Preclinical PET-MRI, a Swedish nationally available imaging platform at Uppsala University, Sweden, financed by the Knut and Alice Wallenberg Foundation. The [^{11}C]PiB synthesis was performed at the Uppsala University Hospital PET centre. Open access funding is provided by Uppsala University. This work was supported by grants from the Swedish Research Council (2021-03524, 2021-01083), Alzheimerfonden, Hjärnfonden, Åhlénstiftelsen, Magnus Bergvalls stiftelse, Stiftelsen för gamla tjänarinnor, Gun and Bertil Stohnes stiftelse and Konung Gustaf V:s och Drottning Victorias frimurarestiftelse. The funding bodies did not take part in design of the study, in collection, analysis or interpretation of data, nor in writing the manuscript.

CONFLICT OF INTEREST STATEMENT

The authors declare that they have no competing interests.

PEER REVIEW

The peer review history for this article is available at https://www.webofscience.com/api/gateway/wos/peer-review/10.1111/jnc.16127.

DATA AVAILABILITY STATEMENT

All data are available upon reasonable request.

ORCID

Stina Syvänen https://orcid.org/0000-0002-8196-4041

REFERENCES

Alafuzoff, I., & Libard, S. (2020). Mixed brain pathology is the most common cause of cognitive impairment in the elderly. *Journal of Alzheimer's Disease*, *78*(1), 453–465.

Budd Haeberlein, S., Aisen, P. S., Barkhof, F., Chalkias, S., Chen, T., Cohen, S., Dent, G., Hansson, O., Harrison, K., von Hehn, C., Iwatsubo, T., Mallinckrodt, C., Mummery, C. J., Muralidharan, K. K., Nestorov, I., Nisenbaum, L., Rajagovindan, R., Skordos, L., Tian, Y., … Sandrock, A. (2022). Two randomized phase 3 studies of aducanumab in early Alzheimer's disease. *The Journal of Prevention of Alzheimer's Disease*, *9*(2), 197–210.

Castellani, R. J., Shanes, E. D., McCord, M., Reish, N. J., Flanagan, M. E., Mesulam, M. M., & Jamshidi, P. (2023). Neuropathology of anti-amyloid-β immunotherapy: A case report. *Journal of Alzheimer's Disease*, *93*(2), 803–813.

Clark, C. M., Schneider, J. A., Bedell, B. J., Beach, T. G., Bilker, W. B., Mintun, M. A., Pontecorvo, M. J., Hefti, F., Carpenter, A. P., Flitter, M. L., Krautkramer, M. J., Kung, H. F., Coleman, R. E., Doraiswamy, P. M., Fleisher, A. S., Sabbagh, M. N., Sadowsky, C. H., Reiman, E. P., Zehntner, S. P., … AV45-A07 Study Group. (2011). Use of florbetapir-PET for imaging beta-amyloid pathology. *Journal of the American Medical Association*, *305*(3), 275–283.

Englund, H., Sehlin, D., Johansson, A. S., Nilsson, L. N., Gellerfors, P., Paulie, S., Lannfelt, L., & Pettersson, F. E. (2007). Sensitive ELISA detection of amyloid-β protofibrils in biological samples. *Journal of Neurochemistry*, *103*(1), 334–345.

Fang, X. T., Hultqvist, G., Meier, S. R., Antoni, G., Sehlin, D., & Syvanen, S. (2019). High detection sensitivity with antibody-based PET radioligand for amyloid β in brain. *NeuroImage*, *184*, 881–888.

Fang, X. T., Sehlin, D., Lannfelt, L., Syvanen, S., & Hultqvist, G. (2017). Efficient and inexpensive transient expression of multispecific multivalent antibodies in Expi293 cells. *Biological Procedures Online*, *19*, 11.

Frieg, B., Gremer, L., Heise, H., Willbold, D., & Gohlke, H. (2020). Binding modes of thioflavin T and Congo red to the fibril structure of amyloid-β (1–42). *Chemical Communications*, *56*(55), 7589–7592.

Gustavsson, T., Metzendorf, N. G., Wik, E., Roshanbin, S., Julku, U., Chourlia, A., Nilsson, P., Andersson, K. G., Laudon, H., Hultqvist, G., Syvänen, S., & Sehlin, D. (2023). Long-term effects of immunotherapy with a brain penetrating Aβ antibody in a mouse model of Alzheimer's disease. *Alzheimer's Research & Therapy*, *15*(1), 90.

Gustavsson, T., Syvanen, S., O'Callaghan, P., & Sehlin, D. (2020). SPECT imaging of distribution and retention of a brain-penetrating bispecific amyloid-β antibody in a mouse model of Alzheimer's disease. *Translational Neurodegeneration*, *9*(1), 37.

Ikonomovic, M. D., Buckley, C. J., Abrahamson, E. E., Kofler, J. K., Mathis, C. A., Klunk, W. E., & Farrar, G. (2020). Post-mortem analyses of PiB and flutemetamol in diffuse and cored amyloid-beta plaques in Alzheimer's disease. *Acta Neuropathologica*, *140*(4), 463–476.

Ikonomovic, M. D., Klunk, W. E., Abrahamson, E. E., Mathis, C. A., Price, J. C., Tsopelas, N. D., Lopresti, B. J., Ziolko, S., Bi, W., Paljug, W. R., Debnath, M. L., Hope, C. E., Isanski, B. A., Hamilton, R. L., & DeKosky, S. T. (2008). Post-mortem correlates of in vivo PiB-PET amyloid imaging in a typical case of Alzheimer's disease. *Brain*, *131*(Pt 6), 1630–1645.

Liu, E., Schmidt, M. E., Margolin, R., Sperling, R., Koeppe, R., Mason, N. S., Klunk, W. E., Mathis, C. A., Salloway, S., Fox, N. C., Hill, D. L., Les, A. S., Collins, P., Gregg, K. M., di, J., Lu, Y., Tudor, I. C., Wyman, B. T., Booth, K., … Good, S. (2015). Amyloid-β 11C-PiB-PET imaging results from 2 randomized bapineuzumab phase 3 AD trials. *Neurology*, *85*(8), 692–700.

Lord, A., Englund, H., Söderberg, L., Tucker, S., Clausen, F., Hillered, L., Gordon, M., Morgan, D., Lannfelt, L., Pettersson, F. E., & Nilsson, L. N. G. (2009). Amyloid-β protofibril levels correlate with spatial learning in Arctic Alzheimer's disease transgenic mice. *The FEBS Journal*, *276*(4), 995–1006.

Lord, A., Gumucio, A., Englund, H., Sehlin, D., Sundquist, V. S., Söderberg, L., Möller, C., Gellerfors, P., Lannfelt, L., Pettersson, F. E., & Nilsson,

L. N. G. (2009). An amyloid-β protofibril-selective antibody prevents amyloid formation in a mouse model of Alzheimer's disease. *Neurobiology of Disease*, *36*(3), 425–434.

Lowe, S. L., Duggan Evans, C., Shcherbinin, S., Cheng, Y. J., Willis, B. A., Gueorguieva, I., Lo, A. C., Fleisher, A. S., Dage, J. L., Ardayfio, P., Aguiar, G., Ishibai, M., Takaichi, G., Chua, L., Mullins, G., & Sims, J. R. (2021). Donanemab (LY3002813) phase 1b study in Alzheimer's disease: Rapid and sustained reduction of brain amyloid measured by florbetapir F18 imaging. *The Journal of Prevention of Alzheimer's Disease*, *8*(4), 414–424.

Magnusson, K., Sehlin, D., Syvänen, S., Svedberg, M. M., Philipson, O., Söderberg, L., Tegerstedt, K., Holmquist, M., Gellerfors, P., Tolmachev, V., Antoni, G., Lannfelt, L., Hall, H., & Nilsson, L. N. G. (2013). Specific uptake of an amyloid-β protofibril-binding antibody-tracer in AβPP transgenic mouse brain. *Journal of Alzheimer's Disease*, *37*(1), 29–40.

Meier, S. R., Sehlin, D., Hultqvist, G., & Syvanen, S. (2021). Pinpointing brain TREM2 levels in two mouse models of Alzheimer's disease. *Molecular Imaging and Biology*, *23*, 665–675.

Meier, S. R., Sehlin, D., Roshanbin, S., Falk, V. L., Saito, T., Saido, T. C., Neumann, U., Rokka, J., Eriksson, J., & Syvänen, S. (2022). ^{11}C-PiB and ^{124}I-antibody PET provide differing estimates of brain amyloid-β after therapeutic intervention. *Journal of Nuclear Medicine*, *63*(2), 302–309.

Meier, S. R., Syvänen, S., Hultqvist, G., Fang, X. T., Roshanbin, S., Lannfelt, L., Neumann, U., & Sehlin, D. (2018). Antibody-based in vivo PET imaging detects amyloid-β reduction in Alzheimer transgenic mice after BACE-1 inhibition. *Journal of Nuclear Medicine*, *59*(12), 1885–1891.

Mishra, S. K., Yamaguchi, Y., Higuchi, M., & Sahara, N. (2021). Pick's tau fibril shows multiple distinct PET probe binding sites: Insights from computational modelling. *International Journal of Molecular Sciences*, *22*(1), 349.

Nelissen, N., van Laere, K., Thurfjell, L., Owenius, R., Vandenbulcke, M., Koole, M., Bormans, G., Brooks, D. J., & Vandenberghe, R. (2009). Phase 1 study of the Pittsburgh compound B derivative 18F-flutemetamol in healthy volunteers and patients with probable Alzheimer disease. *Journal of Nuclear Medicine*, *50*(8), 1251–1259.

Peccati, F., Pantaleone, S., Riffet, V., Solans-Monfort, X., Contreras-García, J., Guallar, V., & Sodupe, M. (2017). Binding of Thioflavin T and related probes to polymorphic models of amyloid-β fibrils. *The Journal of Physical Chemistry. B*, *121*(38), 8926–8934.

Plowey, E. D., Bussiere, T., Rajagovindan, R., Sebalusky, J., Hamann, S., von Hehn, C., Castrillo-Viguera, C., Sandrock, A., Budd Haeberlein, S., van Dyck, C. H., & Huttner, A. (2022). Alzheimer disease neuropathology in a patient previously treated with aducanumab. *Acta Neuropathologica*, *144*(1), 143–153.

Rinne, J. O., Brooks, D. J., Rossor, M. N., Fox, N. C., Bullock, R., Klunk, W. E., Mathis, C. A., Blennow, K., Barakos, J., Okello, A. A., de Llano, S. R. M., Liu, E., Koller, M., Gregg, K. M., Schenk, D., Black, R., & Grundman, M. (2010). 11C-PiB PET assessment of change in fibrillar amyloid-β load in patients with Alzheimer's disease treated with bapineuzumab: A phase 2, double-blind, placebo-controlled, ascending-dose study. *Lancet Neurology*, *9*(4), 363–372.

Rofo, F., Metzendorf, N. G., Saubi, C., Suominen, L., Godec, A., Sehlin, D., Syvänen, S., & Hultqvist, G. (2022). Blood-brain barrier penetrating neprilysin degrades monomeric amyloid-β in a mouse model of Alzheimer's disease. *Alzheimer's Research & Therapy*, *14*(1), 180.

Roshanbin, S., Xiong, M., Hultqvist, G., Söderberg, L., Zachrisson, O., Meier, S., Ekmark-Lewén, S., Bergström, J., Ingelsson, M., Sehlin, D., & Syvänen, S. (2022). In vivo imaging of alpha-synuclein with antibody-based PET. *Neuropharmacology*, *208*, 108985.

Rowe, C. C., Ackerman, U., Browne, W., Mulligan, R., Pike, K. L., O'Keefe, G., Tochon-Danguy, H., Chan, G., Berlangieri, S. U., Jones, G., Dickinson-Rowe, K. L., Kung, H. P., Zhang, W., Kung, M. P., Skovronsky, D., Dyrks, T., Holl, G., Krause, S., Friebe, M., … Villemagne, V. L. (2008). Imaging of amyloid beta in Alzheimer's disease with 18F-BAY94-9172, a novel PET tracer: Proof of mechanism. *Lancet Neurology*, *7*(2), 129–135.

Sehlin, D., Fang, X. T., Cato, L., Antoni, G., Lannfelt, L., & Syvanen, S. (2016). Antibody-based PET imaging of amyloid β in mouse models of Alzheimer's disease. *Nature Communications*, *7*, 10759.

Sehlin, D., & Syvanen, S. (2019). Engineered antibodies: New possibilities for brain PET? *European Journal of Nuclear Medicine and Molecular Imaging*, *46*(13), 2848–2858.

Sevigny, J., Chiao, P., Bussière, T., Weinreb, P. H., Williams, L., Maier, M., Dunstan, R., Salloway, S., Chen, T., Ling, Y., O'Gorman, J., Qian, F., Arastu, M., Li, M., Chollate, S., Brennan, M. S., Quintero-Monzon, O., Scannevin, R. H., Arnold, H. M., … Sandrock, A. (2016). The antibody aducanumab reduces Aβ plaques in Alzheimer's disease. *Nature*, *537*(7618), 50–56.

Sims, J. R., Zimmer, J. A., Evans, C. D., Lu, M., Ardayfio, P., Sparks, J., Wessels, A. M., Shcherbinin, S., Wang, H., Monkul Nery, E. S., Collins, E. C., Solomon, P., Salloway, S., Apostolova, L. G., Hansson, O., Ritchie, C., Brooks, D. A., Mintun, M., Skovronsky, D. M., … Zboch, M. (2023). Donanemab in early symptomatic Alzheimer disease: The TRAILBLAZER-ALZ 2 randomized clinical trial. *Journal of the American Medical Association*, *330*(6), 512–527.

Söderberg, L., Johannesson, M., Nygren, P., Laudon, H., Eriksson, F., Osswald, G., Möller, C., & Lannfelt, L. (2023). Lecanemab, aducanumab, and gantenerumab—Binding profiles to different forms of amyloid-β might explain efficacy and side effects in clinical trials for Alzheimer's disease. *Neurotherapeutics*, *20*(1), 195–206.

Solbach, C., Uebele, M., Reischl, G., & Machulla, H. J. (2005). Efficient radiosynthesis of carbon-11 labelled uncharged Thioflavin T derivatives using [^{11}C]methyl triflate for β-amyloid imaging in Alzheimer's disease with PET. *Applied Radiation and Isotopes*, *62*(4), 591–595.

Swanson, J. D., Zhang, Y., Dhadda, S., Wang, J., Kaplow, J., Lai, R. Y. K., Lannfelt, L., Bradley, H., Rabe, M., Koyama, A., Reyderman, L., Berry, D. A., Berry, S., Gordon, R., Kramer, L. D., & Cummings, J. L. (2021). A randomized, double-blind, phase 2b proof-of-concept clinical trial in early Alzheimer's disease with lecanemab, an anti-Aβ protofibril antibody. *Alzheimer's Research & Therapy*, *17*(11), 80.

Syvänen, S., Hultqvist, G., Gustavsson, T., Gumucio, A., Laudon, H., Söderberg, L., Ingelsson, M., Lannfelt, L., & Sehlin, D. (2018). Efficient clearance of Aβ protofibrils in AβPP-transgenic mice treated with a brain-penetrating bifunctional antibody. *Alzheimer's Research & Therapy*, *10*(1), 49.

Syvänen, S., Meier, S. R., Roshanbin, S., Xiong, M., Faresjö, R., Gustavsson, T., Bonvicini, G., Schlein, E., Aguilar, X., Julku, U., Eriksson, J., & Sehlin, D. (2022). PET imaging in preclinical anti-Aβ drug development. *Pharmaceutical Research*, *39*(7), 1481–1496.

Tao, Y., Xia, W., Zhao, Q., Xiang, H., Han, C., Zhang, S., Gu, W., Tang, W., Li, Y., Tan, L., Li, D., & Liu, C. (2023). Structural mechanism for specific binding of chemical compounds to amyloid fibrils. *Nature Chemical Biology*, *19*(10), 1235–1245.

Tucker, S., Möller, C., Tegerstedt, K., Lord, A., Laudon, H., Sjödahl, J., Söderberg, L., Spens, E., Sahlin, C., Waara, E. R., Satlin, A., Gellerfors, P., Osswald, G., & Lannfelt, L. (2015). The murine version of BAN2401 (mAb158) selectively reduces amyloid-β protofibrils in brain and cerebrospinal fluid of tg-ArcSwe mice. *Journal of Alzheimer's Disease*, *43*(2), 575–588.

van Dyck, C. H., Swanson, C. J., Aisen, P., Bateman, R. J., Chen, C., Gee, M., Kanekiyo, M., Li, D., Reyderman, L., Cohen, S., Froelich, L., Katayama, S., Sabbagh, M., Vellas, B., Watson, D., Dhadda, S., Irizarry, M., Kramer, L. D., & Iwatsubo, T. (2023). Lecanemab in early Alzheimer's disease. *The New England Journal of Medicine*, *388*(1), 9–21.

Ye, L., Velasco, A., Fraser, G., Beach, T. G., Sue, L., Osredkar, T., Libri, V., Spillantini, M. G., Goedert, M., & Lockhart, A. (2008). In vitro high affinity alpha-synuclein binding sites for the amyloid imaging agent PIB are not matched by binding to Lewy bodies in postmortem human brain. *Journal of Neurochemistry*, *105*(4), 1428–1437.

Zielinski, M., Peralta Reyes, F. S., Gremer, L., Schemmert, S., Frieg, B., Schäfer, L. U., Willuweit, A., Donner, L., Elvers, M., Nilsson, L. N. G., Syvänen, S., Sehlin, D., Ingelsson, M., Willbold, D., & Schröder, G. F. (2023). Cryo-EM of Aβ fibrils from mouse models find tg-APP(ArcSwe) fibrils resemble those found in patients with sporadic Alzheimer's disease. *Nature Neuroscience*, *26*(12), 2073–2080.

SUPPORTING INFORMATION

Additional supporting information can be found online in the Supporting Information section at the end of this article.

How to cite this article: Xiong, M., Dahlén, A., Roshanbin, S., Wik, E., Aguilar, X., Eriksson, J., Sehlin, D., & Syvänen, S. (2024). Antibody engagement with amyloid-beta does not inhibit [^{11}C]PiB binding for PET imaging. *Journal of Neurochemistry*, *168*, 2601–2610. https://doi.org/10.1111/jnc.16127